Localized chemical release from an artificial synapse chip

Mark C. Peterman*†, Jaan Noolandi‡, Mark S. Blumenkranz‡, and Harvey A. Fishman‡

*Department of Applied Physics, Stanford University, Stanford, CA 94305-4090; and ‡Department of Ophthalmology, Stanford University, Stanford, CA 94305-5308

Edited by Robert S. Langer, Massachusetts Institute of Technology, Cambridge, MA, and approved May 24, 2004 (received for review March 24, 2004)

A device that releases chemical compounds in small volumes and at multiple, well defined locations would be a powerful tool for clinical therapeutics and biological research. Many biomedical devices such as neurotransmitter-based prostheses or drug delivery devices require precise release of chemical compounds. Additionally, the ability to control chemical gradients will have applications in basic research such as studies of cell microenvironments, stem cell niches, metaplasia, or chemotaxis. We present such a device with repeatable delivery of chemical compounds at multiple locations on a chip surface. Using electroosmosis to drive flow through microfluidic channels, we pulse minute quantities of a bradykinin solution through four 5-μm apertures onto PC12 cells and show stimulation of individual cells using a Ca^{2+}-sensitive fluorescent dye. We also present basic computational results with experimental verification of both fluid ejection and fluid withdrawal by imaging pH changes by using a fluorescent dye. This ''artificial synapse chip'' is a prototype neural interface that introduces a new paradigm for neural stimulation, with eventual application in treating macular degeneration and other neurological disorders.

Devices that can repeatedly release chemical compounds in small volumes and at multiple locations would be powerful clinical and laboratory tools. Some clinical therapeutics such as implantable drug-delivery devices (1) and neurotransmitter-based neural prostheses (2, 3) require the controlled release of chemical compounds. However, many of the current devices have limited control or repeatability. In addition, basic research requiring control over chemical gradients, such as studies of cell microenvironments (4–6), stem cell niches (7, 8), metaplasia (9), or chemotaxis (10–12), can benefit from a general chemical-release device. In these areas of study, the local cellular environment plays a significant role in function; a device that enables control over cellular microenvironments may prove to be a powerful research tool.

In this article, we present such a device, with repeatable delivery of chemical compounds at multiple locations on a chip surface. The device consists of an array of four 5-μm circular apertures, each connected to a microfluidic channel. Using electroosmosis to drive fluid flow, we show ejection of minute quantities of a bradykinin solution through these apertures onto PC12 cells; with a Ca^{2+}-sensitive fluorescent dye, we measure stimulation of individual cells. In addition, we use a finite element model to derive basic computational results and provide experimental verification of both fluid ejection and fluid withdrawal through imaging pH changes of a fluorescent dye.

We labeled our device an ''artificial synapse chip.'' We built the device for application to a neurotransmitter-based retinal prosthesis, a device that, in essence, mimics a synapse by controlled, repeatable release of neurotransmitters. The use of neurotransmitters for stimulation instead of electric fields provides a unique approach to retinal prostheses. Unlike electric field stimulation, neurotransmitter stimulation can maintain many of the natural signaling pathways in the retina such as the on/off-center (13) pathway or α-amino-3-hydroxy-5-methyl-4-isoxazolepropionic acid/kinate-based (14) temporal pathways. To this end of mimicking synaptic transmission, our device releases small quantities of neurostimulant solution at well defined locations.

Materials and Methods

Device Fabrication. The basic device was fabricated as described (2, 15). Low-stress silicon nitride (1.6 μm) was deposited on double-polished silicon wafers. The silicon nitride was patterned by using photolithography and reactive ion etching to produce the 2×2 array of 5-μm circular apertures (125 μm centers) on the front side of the wafer and square regions as a through-wafer etch mask on the back side of the wafer. Gold electrodes (100 nm Ti and 150 nm Au) for controlling the electroosmotic flow (EOF) were deposited and patterned by liftoff. Then, the silicon-nitride membranes were released by using an anisotropic silicon etch (tetramethylammonium hydroxide, 95°C, 5–6 h), providing access to both sides of the apertures.

The microfluidic channels were formed from patterned SU-8 photoresist (Microchem, Newton, MA). First, the wafers were dehydration-baked at 150°C for 4 h to improve SU-8 adhesion. The SU-8 was applied to the wafer 25 μm thick, per manufacturer specifications. To drive out solvent before lithography, the wafers were carefully soft-baked: a slow temperature ramp (1°C per min) from room temperature to 85°C, held at 85°C for 1 h, and then cooled at 1°C per min. We observed that fast ramp speeds to the recommended bake temperature break the thin silicon-nitride membrane, presumably because of differences in the coefficients of thermal expansion. After baking, the SU-8 was exposed, creating channels aligned to the apertures. A hard bake was performed before development, with slow ramp speeds as with the soft-bake process.

Microscopy and Imaging. Changes in fluorescent levels were observed with a Nikon E800 ($\times$10 dipping objective, 0.30 numerical aperture), a Nikon PCM 2000 confocal unit, and a Sony DXC-390 charge-coupled device color camera. For confocal imaging (of fluorescein bubbles), two lasers were used to excite the Fluo-4 (Ar ion, 488 nm) and Texas red (HeNe, 543 nm). Images were sampled simultaneously by using two photomultiplier tubes (515/30 bandpass and 605/32 bandpass filters) and analyzed by using SIMPLEPCI (Compix, Cranberry Township, PA). The Sony camera was used in conjunction with a mercury arc lamp for standard fluorescence imaging of fluid flow through the bent channels.

Electric Field-Driven Fluid Ejection. The chips were mounted in an acrylic holder consisting of an acrylic base plate with fluid access holes (see Fig. 1) and a capping plate with a central hole as a fluid bath. The chip was aligned by using a piece of thin, transparent silicone rubber (polydimethylsiloxane) as a gasket. Thin strips of

This paper was submitted directly (Track II) to the PNAS office.

Abbreviation: EOF, electroosmotic flow.

†To whom correspondence should be sent at the present address: Alces Technology, Inc., P.O. Box 11180, Jackson, WY 83002-1180. E-mail: peterman@alcestech.com.

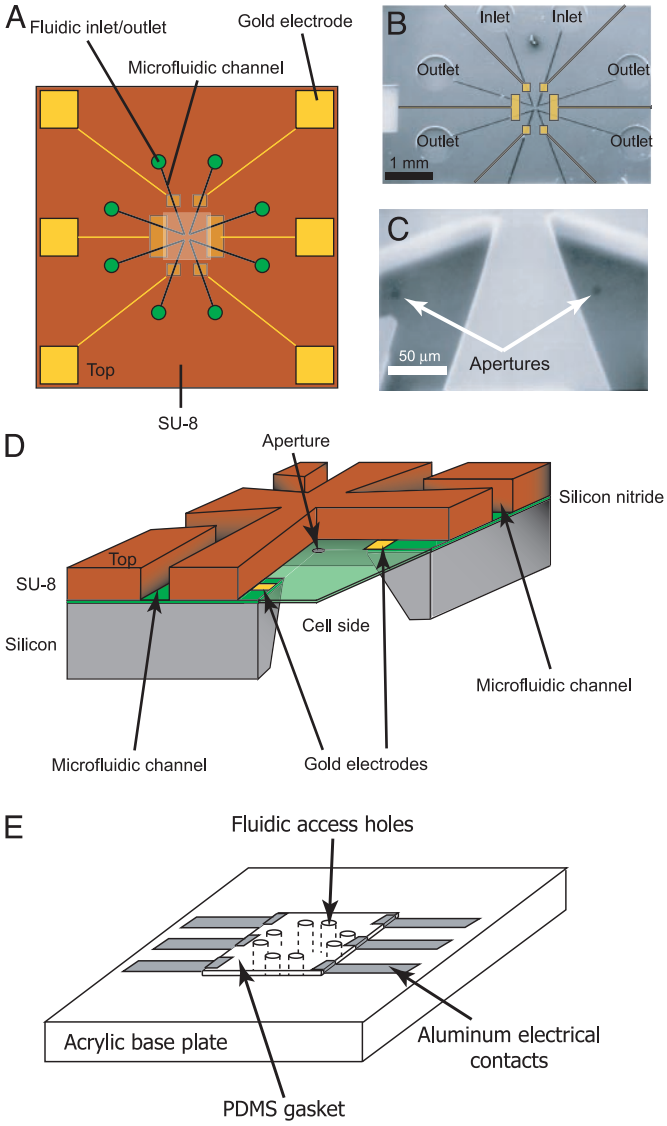

Fig. 1. The artificial synapse chip. (*A*) Top view schematic of the multisite stimulation device (8 × 8 mm). The active area is on the bottom of the device. (*B*) Scanning electron micrograph of the device. (*C*) Higher-magnification scanning electron micrograph of the channel corners. The apertures are visible inside the channels, as indicated by the arrows. (*D*) Cutout schematic at the center of the device. The silicon and SU-8 layers have been removed from one corner, providing a view of the anisotropically etched well in which cells are cultured. (*E*) Illustration of the acrylic holder used to interface the devices. The polydimethylsiloxane gasket, acrylic base plate, and aluminum foil electrical contacts are shown.

aluminum foil for electrical contacts to the gold pads were placed on the polydimethylsiloxane gasket before the chip was aligned. Once the chip was mounted in the holder, fluid was loaded into the channels through access holes in the acrylic block by using a pipettor. The holder was placed on a microscope stage, the fluidic bath was filled with an appropriate solution (e.g., Ringer's solution for PC12 cells), and electrical contact was made with alligator clips to the power supply. The electrical signals were supplied through a four-channel digital-to-analog converter (ITC18, Instrutech, Port Washington, NY) controlled via IGOR (WaveMetrics, Lake Oswego, OR). Custom functions written within IGOR drove the channels with a single period sine wave of varying amplitude and/or period.

Numerical Simulations. The numerical simulations were carried out on a Pentium IV-class personal computer with 1.5 GB of RAM and running WINDOWS 2000. The equations were solved by using a finite element method in FEMLAB (Comsol, Burlington, MA), which runs within MATLAB (Mathworks, Natick, MA). The software was supplied with the Navier–Stokes equation (as in ref. 16) in addition to the electric field due to the applied potential (φ) and the electric double layer (ψ). Diffusion- and convection-driven concentration changes were also solved. Additional results are explored in ref. 16.

Chip Treatment. Because the PC12 cells used here do not readily adhere to silicon nitride, we treated the chips before seeding with cells (17). A droplet of poly(D-lysine) at 50 μg/ml was placed over the silicon-nitride window for 30 min at room temperature. After rinsing the devices in PBS, laminin was applied at 2–5 μg/ml in PBS for 8 h in an incubator (37°C, 6.5% CO_2). The chips were rinsed in PBS and ready for use.

Fluorescent Dye Loading and Measurement. Measurement of bradykinin stimulation was accomplished by observing changes in intracellular Ca^{2+} levels by using Fluo-4 (Molecular Probes). The cells were loaded with Fluo-4 per manufacturer specifications in a Ringer's solution (135 mM NaCl/5 mM KCl/10 mM D-glucose/2 mM $MgCl_2$/2 mM $CaCl_2$/10 mM Hepes, pH 7.2). The stimulating solution was a mixture of bradykinin (Sigma), Ringer's solution, and sulforhodamine 101 or fluorescein (Sigma). Bradykinin was reconstituted in Ringer's at 1 mg/ml (1 mM) and then diluted to 10 μM. Sulforhodamine was reconstituted in DMSO at 8 mM and added to the stimulating solution to yield a final concentration of 4–8 μM.

Results and Discussion

The basic component in our 8 × 8-mm device was a small, circular aperture in the side of a microfluidic channel. Using standard microfabrication techniques, we deposited a thin layer of silicon nitride (1.6 μm thick) on a silicon wafer. Through the silicon nitride we etched four circular apertures in a 2 × 2 array (5 μm diameter, 125 μm center to center). We then anisotropically etched through the silicon wafer, creating a thin, free-standing membrane ≈350 μm on a side. Channels were created by lithographically patterning 25-μm-deep SU-8 photoresist over the apertures (Fig. 1*A*). The 50-μm-wide channels were designed with a bend to allow each channel to overlay a single aperture.

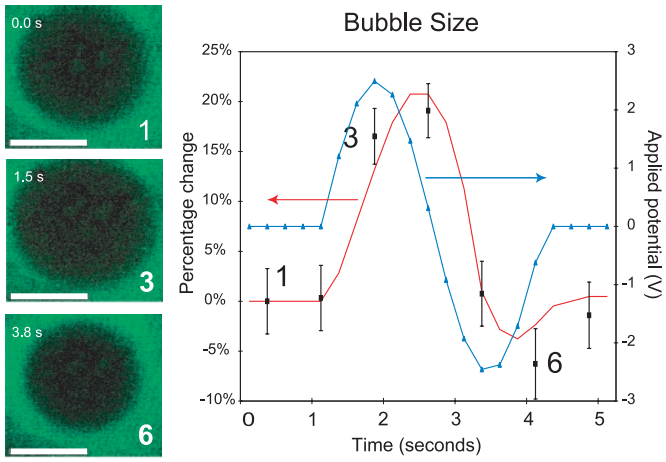

Fig. 2. Fluorescein bubble size variations as a function of time. (*Left*) Experimental scanning confocal micrographs at 0.0, 1.5, and 3.8 sec (n = 11). The applied potential began at 1.0 sec. (Scale bar, 25 μm.) (*Right*) Computational model for concentration above aperture in comparison with experimental data (black squares are data, and the solid red line is the model). The applied pulse is included on the plot in blue. [Reproduced with permission from ref. 16 (copyright 2004, American Chemical Society).]

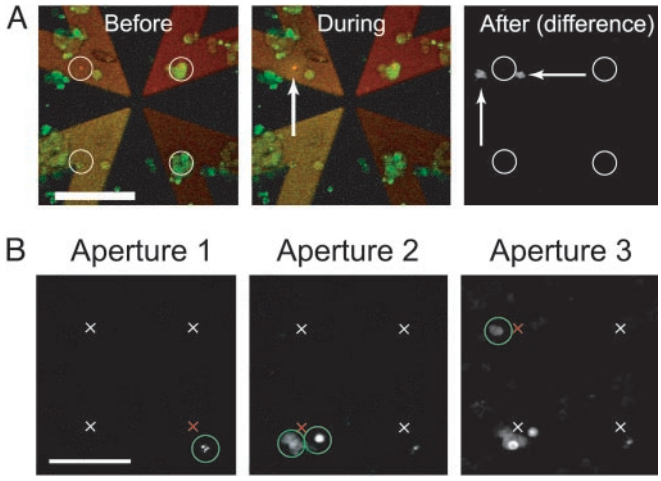

Fig. 3. Sequential, multisite PC12 stimulation. (*A*) Single aperture PC12 stimulation. Scanning confocal micrographs of the device with PC12 cells before (*Left*), during (*Center*), and after (*Right*) stimulation. The channels were filled with combinations of Texas red and fluorescein dyes. The 20-μm circles are concentric with the 5-μm apertures. A fluid puff is visible at the active aperture, as indicated by the arrow in the middle frame. The last frame shows stimulated cells after a background subtraction. (Scale bar, 100 μm.) (*B*) Sequential, multisite PC12 stimulation. The frames display cell stimulation during sequential activation of three channels. The crosses indicate the location of the apertures, with red indicating the active aperture. The green circles are visual guides to indicate stimulated PC12 cells. A background from before stimulation was subtracted from each frame. (Scale bar, 100 μm.)

The bend provides enough room for inlet and outlet connections to each channel. Gold electrodes for controlling EOF were patterned inside the channels, with two common grounds and four control lines (shown in Fig. 1 *B* and *C*). A cutout view of the device is shown in Fig. 1*D*. Although the dimensions of this device were larger than native synaptic connections, scaling to synaptic dimensions ($\approx$1 μm per stimulation site) will not be difficult with microfabrication.

We used EOF to drive the fluid through the channels. Electroosmosis is the bulk flow of fluid due to an applied electric field. At the solid–liquid interface along the channel wall, an electric double layer forms, with one charged layer fixed to the channel wall and the other charged layer mobile in the solution. An applied electric field parallel to this mobile layer drives the ions down the channel. In low Reynolds' number flow (i.e., highly viscous), such as that in our channels ($Re < 0.01$), this flow entrains the bulk solution, resulting in flow through the channel. This effect can be modeled by solving the Navier–Stokes equation with an extra force term (18),

$$\rho\left[\frac{\partial \mathbf{v}}{\partial t} + (\mathbf{v}\cdot\nabla)\mathbf{v}\right] = -\nabla p + \mu\nabla^2\mathbf{v} + \varepsilon\varepsilon_0\kappa^2\psi\nabla\varphi, \qquad [1]$$

where ρ is the density of water, μ is the viscosity of water, ε is the dielectric constant, p is the pressure, κ describes the electric double-layer thickness, ψ is the potential due to the electric double layer, φ is the applied potential, and $\mathbf{v}$ is the velocity.

The channels were filled with an acidic fluorescein solution to observe fluid flow and to test the effects of a time-varying EOF. Fluorescein is a popular fluorescent dye because of its excellent quantum yield at high (basic) pH. However, in acidic conditions, the fluorescence is greatly reduced. When we fill the channel with an acidic fluorescein solution (pH $\approx$3), the channel appears dark under scanning confocal microscopy. As the fluorescein solution flows through the aperture, it mixes with the neutral pH bath (pH 7.4) and fluoresces. This mixing is visible as a circle of dark solution (a "bubble") with a bright rim, centered on the aperture. In the center of the bubble, the solution is too acidic to fluoresce, but diffusional mixing increases the pH radially outward from the aperture, leading to fluorescence. As we applied a time-varying potential to the channel (sine wave, $\pm$2.5 V, 3.125-sec period), fluid was first ejected from the aperture, increasing the size of the bubble, and then withdrawn back into the aperture, decreasing the size of the bubble (16). Using the image-analysis software to increase the contrast and find a threshold value in fluorescence intensity, we measured the relative size of the bubble as a function of time. These data are shown in Fig. 2, in which the size of 11 different bubbles was normalized and averaged. When the direction of the field was switched (negative first), the bubble first shrank and then grew.

We solved Eq. **1** by using a finite element model to develop a computational expectation for this system. In this numerical simulation, we modeled the diffusion- and convection-driven

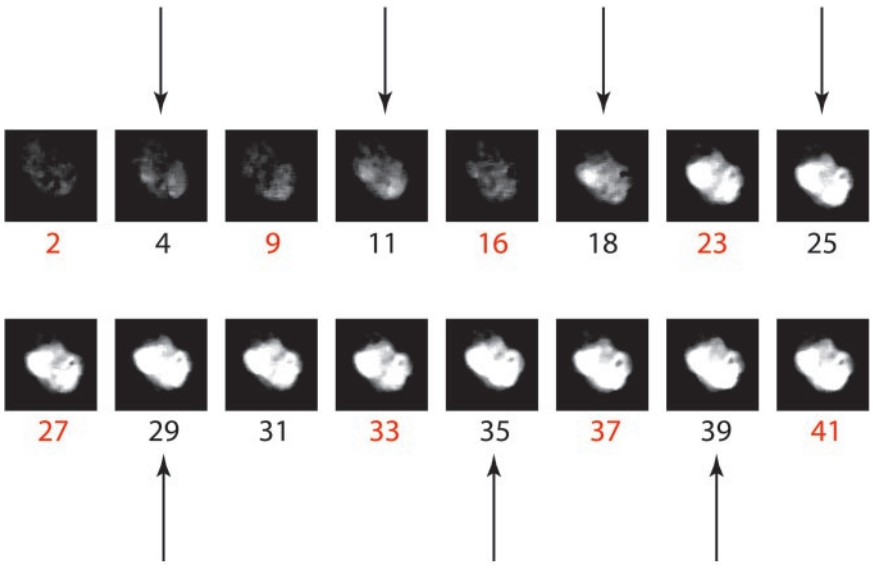

Fig. 4. Repeat stimulation of two PC12 cells. The frame numbers are indicated, with red indicating the frame at which stimulation is activated. The arrows indicate the frames at which the stimulation is a maximum, always two frames after stimulation.

concentration change above the aperture. To compare the model with experimental data, we plotted the position at which the system reaches an arbitrary concentration as a function of time. As can be seen in Fig. 2 *Right*, the model predicts the observed behavior. The ability to eject and withdraw fluid is important. Ejected fluid will eventually saturate the bath unless the bath volume is very large or there is some form of uptake. For retinal prostheses, this excess fluid may lead to two difficulties: (*i*) extra fluid under the retina can result in a retinal detachment; and (*ii*) high concentrations of excess glutamate can result in neurodegeneration through excitotoxicity (19). Moreover, diffusion through the apertures leads to constant loss from the channel into the bath. The ability to withdraw fluid can limit the number of molecules ejected into the bath, potentially comparable with the 10^4 molecules released during synaptic transmission.

To demonstrate the use of this device in biological systems, we cultured cells from the PC12 cell line on the surface of the chip. The silicon-nitride surface was first treated with poly(D-lysine) and laminin to promote cell growth. PC12 cells changed their intercellular Ca^{2+} levels after a bradykinin stimulus (20). We filled the channels with a bradykinin solution (10 μM in a Ringer's solution) mixed with the fluorescent dyes Texas red and/or fluorescein for visualization (Fig. 3*A Left*). The Fluo-4 within the PC12 cells weakly fluoresced green before application of bradykinin. When we activated the channel, a small amount of fluid was seen to eject from the aperture (Fig. 3*A Center*), leading to stimulation of the two PC12 cells nearest the aperture ($\approx$25 μm from the aperture to the cells). There were many other cells in the image, but because of the limited amount of ejected fluid, only the region nearest the aperture reached a concentration high enough to stimulate the PC12s (Fig. 3*A Right*).

More importantly, we can stimulate sequentially by using different apertures. In Fig. 3*B* we show stimulation at three different sites. Beginning at the lower right, we activated three channels sequentially in a clockwise direction (at 6.6, 19.9, and 42.0 sec) by using a digital-to-analog converter. At each time point, stimulation was limited to 25 μm from the aperture. The time between stimulation events from different channels was long; this delay is due to the rather slow dynamics of PC12 cells and manual control of the system driving the channels. The channels were controlled manually by running the appropriate code within IGOR. With a device under this type of control, a researcher can observe the system, choose the region to stimulate, and then release a compound within that region. Subsequently, other regions can be stimulated with different concentrations or compounds, all within the same sample.

Finally, in Fig. 4, we show repeat stimulation of PC12 cells. In these data, two cells grew directly over the aperture. When we applied the first pulse (frame 2), the cells were seen to brighten slightly (frame 4) and then dim. A second pulse was applied, brightening the cells again. As we continued the cycle of pulsing stimulant onto the cells at a more rapid pace, the cells continued a cycle of brightening and dimming, each time dimming less than they brightened, finally reaching full stimulation. Maximum stimulation occurs between the first and second frames after channel activation, or between 2.2 and 4.4 sec. From the bubble dynamics, we note that the applied pulse reached its maximum ejection $\approx$1.5 sec after initiation. Additionally, PC12 cells required 1.5 sec to respond to a stimulus (21, 22). Thus, we would expect PC12 cells to respond 3 sec after activation, which would be observed at the second frame after activation. We consistently see cell stimulation two frames after channel activation. If the stimulation were caused by the electric field near the aperture, we would expect the maximum stimulation to occur $<$1 sec after activation ($\pi/2$ into the pulse, or 0.8 sec).

Conclusions

We have shown ejection and withdrawal of fluid onto a biological sample by using electroosmosis as the driving force, in effect mimicking the active component of a synapse. Electroosmosis is very convenient because of its simplicity (no moving parts) and low power requirements. Considering only the power required for EOF (23) (i.e., ignoring resistances other than the solution in the channel), we estimate that this device consumes 20 μW; shrinking the dimensions for a high-resolution prosthesis (2.5 $\times$ 2.5-μm channels, 10 μm between 1-μm apertures, interdigitated electrodes 10 μm apart), we can reduce the power expenditure to 2 nW per channel. This analysis ignores other power requirements such as control electronics, which will be a significant source of heat generation and power consumption. However, thermal damage to the retina can be avoided by moving the control electronics away from the retina, leaving only the low-power microfluidic components in contact with the neural tissue (24).

Although our objective for the artificial synapse chip is a retinal prosthesis, the applications for this technology are rather wide-ranging. For example, recording electrodes could be deposited around the aperture, allowing for simultaneous electrical recording and chemical stimulation of neural cells or tissue slices. The present device with four apertures could be used to eject four different modulatory molecules on a tissue sample, all within a small lateral or temporal range. Our experimental and numerical results show that a line of apertures in a single channel lead to a concentration gradient of fluid ejected, potentially useful for studying the effects of drug levels or chemotaxis *in vitro*. However, for use as a retinal prosthetic interface, more work is necessary, with the next possible steps being to (*i*) increase the number of apertures, requiring better fluidic interfacing and improved fluidic interconnects, and (*ii*) reduce the device to implantable dimensions, requiring a change in materials.

Device fabrication was performed at the Stanford Nanofabrication Facility. We thank VISX (Santa Clara, CA) for funding this research project.

1. Santini, J. T., Cima, M. J. & Langer, R. (1999) *Nature* **397,** 335–338.
2. Peterman, M. C., Bloom, D. M., Lee, C., Bent, S. F., Marmor, M. F., Blumenkranz, M. S. & Fishman, H. A. (2003) *Invest. Ophthalmol. Visual Sci.* **44,** 3314–3149.
3. Vastag, B. (2002) *J. Am. Med. Assoc.* **288,** 1833–1834.
4. Mahoney, M. & Saltzman, W. (2001) *Nat. Biotechnol.* **19,** 934–939.
5. Liotta, L. & Kohn, E. (2001) *Nature* **411,** 375–379.
6. Monje, M., Mizumatsu, S., Fike, J. & Palmer, T. (2002) *Nat. Med.* **8,** 955–962.
7. Spradling, A., Drummond-Barbosa, D. & Kai, T. (2001) *Nature* **414,** 98–104.
8. Lin, H. (2002) *Nat. Rev. Genet.* **3,** 931–940.
9. Tosh, D. & Slack, J. M. W. (2002) *Nat. Rev. Mol. Cell Biol.* **3,** 187–194.
10. Song, H. J. & Poo, M. M. (2001) *Nat. Cell Biol.* **3,** E81–E88.
11. Bourne, H. R. & Weiner, O. (2002) *Nature* **419,** 21.
12. Ueda, M., Sako, Y., Tanaka, T., Devreotes, P. & Yanagida, T. (2001) *Science* **294,** 864–867.
13. Masland, R. H. (2001) *Nat. Neurosci.* **4,** 877–886.
14. DeVries, S. H. (2000) *Neuron* **28,** 847–856.
15. Peterman, M. C., Ziebarth, J. M., Braha, O., Bayley, H., Fishman, H. A. & Bloom, D. M. (2002) *Biomed. Microdevices* **4,** 231–236.
16. Peterman, M. C., Noolandi, J., Blumenkranz, M. S. & Fishman, H. A. (2004) *Anal. Chem.* **76,** 1850–1856.
17. Hirata, I., Iwata, H., Ismail, A. B. M., Iwasaki, H., Yukimasa, T. & Sugihara, H. (2000) *Jpn. J. Appl. Phys. I* **39,** 6441–6442.
18. Patankar, N. & Hu, H. (1998) *Anal. Chem.* **70,** 1870–1881.
19. Nedergaard, M., Takano, T. & Hansen, A. J. (2002) *Nat. Rev. Neurosci.* **3,** 748–755.
20. Greene, L. A. & Tischler, A. S. (1976) *Proc. Natl. Acad. Sci. USA* **73,** 2424–2428.
21. Bui, J. D., Zelles, T., Lou, H. J., Gallion, V. L., Phillips, M. I. & Tan, W. H. (1999) *J. Neurosci. Methods* **89,** 9–15.
22. Fink, C. C., Slepchenko, B., Moraru, II, Watras, J., Schaff, J. C. & Loew, L. M. (2000) *Biophys. J.* **79,** 163–183.
23. Burgreen, D. & Nakache, F. (1965) *J. Appl. Mech.* **32,** 675–679.
24. Humayun, M. S. (2001) *Trans. Am. Ophthalmol. Soc.* **99,** 271–300.